Journal of Building Engineering 75 (2023) 106949

Contents lists available at ScienceDirect

Journal of Building Engineering

journal homepage: www.elsevier.com/locate/jobe

Effect of artificial interior stone sludge on physicomechanical properties of mortars

G.M. Kim [a, b], Jaesuk Choi [c], Jinho Bang [c], Jongwon Jung [c], S.W. Park [a, **], Beomjoo Yang [c, *]

[a] Mineral Processing & Metallurgy Research Center, Resources Utilization Division, Korea Institute of Geoscience and Mineral Resources, 124 Gwahak-ro, Yuesong-gu, Daejeon 34132, Republic of Korea
[b] Department of Resources Recycling, Korea University of Science and Technology, 217 Gajeong-ro Yuseong-gu, Daejeon, 34113, Republic of Korea
[c] School of Civil Engineering, Chungbuk National University, 1 Chungdae-ro, Seowon- gu, Cheongju, Chungbuk, 28644, Republic of Korea

ARTICLE INFO

Keywords:
Artificial interior stone sludge
Mortars
Compressive strength
Hydration
Fine aggregates

ABSTRACT

Artificial interior stone is a decorative building material, which mostly consists of quartz. Sludge is generated during the stone manufacturing process, and the amount of sludge is increasing due to the high demand; however, most of the generated sludge is disposed of in landfills. In the present study, the effects of the sludge addition on the physicomechanical properties of mortars were investigated via flowability, penetration resistance, mercury intrusion, and compressive strength tests. The independent variable was the replacement ratio of the sludge to the fine aggregate. The test results showed that the addition of the sludge reduced the flowability, and initial and final setting times, while the percentage of the pores involved in the hydrates increased. The compressive strength of mortars with the sludge was improved compared to that of the mortars without the sludge. Quantum chemistry simulations were conducted to understand the strength enhancement mechanism of the specimens, and a straightforward machine learning-based model equation was proposed by applying the experimental variables and measurement results.

1. Introduction

Concrete is the most popular construction material generally consisting of cements, fine and coarse aggregates, and water. This material has various advantages including stable strength evolution and durability, and economic aspects [1]. Furthermore, the material can be readily molded into desired shapes since it retains a plastic state for a sufficient period [2]. However, the cost of concretes has rapidly increased over the past two decades, owing to the increase in the price of raw materials and energy for production, and the high demand [2].

The issues such as sustainability, climate change, clear production, and resource efficiency are also emerging worldwide so that the eco-friendly production and the use of concretes are highly emphasized [3]. Various techniques for the use of industrial wastes as a starting material for synthesizing clinker, a binder material as itself, and alternatives to fine and coarse aggregates for eco-friendly production of concretes have been investigated [4–7]. The production of concretes utilizing industrial wastes is supported by policies in various countries, and the trend is strengthening [7].

* Corresponding author.
** Corresponding author
E-mail addresses: psw1231@kigam.re.kr (S.W. Park), byang@chungbuk.ac.kr (B. Yang).

https://doi.org/10.1016/j.jobe.2023.106949
Received 11 April 2023; Received in revised form 17 May 2023; Accepted 27 May 2023
Available online 29 May 2023

Among the recycling techniques of industrial wastes in the concrete sector, studies on the use of the wastes as an alternative to aggregates have been extensively attempted [7]. In particular, the utilization of various sludges is one of the representative approaches [7]. The type of industrial wastes such as sewage sludge, granite sludge, and steel sludge has a suitable particle size for the application as a fine aggregate [8,9]. Chen et al. reported that the addition of sewage sludge to concretes improved the long-term compressive strength due to the moderate pozzolanic activity [9]. Fontes et al. reported that the replacement of OPC with sewage sludge up to 30% in mortars was capable without a significant reduction in the compressive strength [8]. It was reported that the addition of granite sludge to concretes improved the compressive strength by more than 10% when the replacement ratio to the fine aggregate was approximately 10% [10]. Nakic reported that the use of the type of sludges for concrete production may have the potential for reduction in the global warming potential and conservation of natural aggregates [11].

Meanwhile, an accurate material simulation would enable materials engineering not only to predict the performance but also to help design new construction materials [12,13]. Hence, there have been various studies to predict the performance of construction materials containing waste resources [14]. Hydration characteristics and modeling of municipal solid wastes incineration fly ash-blast furnace slag-cement were carried out [15]. The thermodynamics modeling was adopted to estimate the compressive strength and hydration characteristics, yielding the slag can be activated by chloride and sulfate in fly ash to form ettringite and Friedel's salt. It was also concluded that the maximum volume of ettringite and Friedel's salt is obtained at nearly 0.55 of fly ash proportion. Molecular dynamics (MD) studies were conducted by Han et al. to simulate the interfacial strengthening mechanism of waste rubber/cement paste using polyvinyl alcohol (PVA) [16]. The transformed characteristics of van der Waals force and electrostatic interaction were modeled by MD simulation, calculating the interfacial adhesion energy between rubber hydrocarbon (RH) and PVA is much higher than that between RH and calcium-silicate-hydrate. Due to the difficulty of reflecting the complex hydration mechanism, research on the data-driven model that can provide further insight into the roles of each variable is also required recently.

In the present study, artificial interior stone (AIS) sludge was utilized as the fine aggregate in mortars. The sludge generated during the manufacturing process of AIS mostly consists of quartz. Herein, the effects of the AIS sludge addition on the physicomechanical properties of mortars were investigated via flowability, penetration resistance, mercury intrusion, and compressive strength tests. The independent variable is the replacement ratio of the sludge to fine aggregates. Density functional theory (DFT) and molecular dynamics (MD) simulations were performed to understand the strength enhancement mechanism of the specimens. Furthermore, a facile machine learning-based model equation was proposed by applying the experimental variables and measurement results.

2. Experimental section

2.1. Raw materials

A binder material used here was ordinary Portland cement (HANIL Cement Co. Ltd., Republic of Korea), and the sand (Jumunsin standard sand, Republic of Korea) was used as a fine aggregate. The SiO_2 content of the standard sand was more than 98%. The AIS sludge was also used as a part of fine aggregate. The water content of the sludge was approximately 27%, and was removed by drying in an oven at 110 ˚C for 24 h. Table 1 showed the chemical composition of OPC and AIS sludge. The sludge was mostly composed of SiO_2 (≈ 97.5%). The shape of the sludge was mostly non-uniform and varied from elliptical to angular. It was far from spherical particles that could help fluidity. In addition, heavy metals for Pb, Cr, Cu, and Cd in the sludge were not eluted, so it was analyzed as environmentally safe. A more detailed analysis result of sludge can be found in literature [17]. Fig. 1 showed the cumulative particle size distribution curves of OPC, standard sand, and AIS sludge. The curve of the AIS sludge was on the far left compared to that of OPC and standard sand, indicating that the sludge in the present study was composed of the smallest particles. The D50 values of OPC, standard sand, and sludge were approximately 8.6 μm and 430 μm, and 5.0 μm, respectively. A Polycarboxylate-type superplasticizer was used when fabricating mortars with AIS sludge (Dongnam Co., Ltd., FLOWMIX 3000 L).

2.2. Sample preparation

Table 2 showed the mix proportion of the mortars with the AIS sludge. Water to cement ratio was 0.41, and the content of the superplasticizer was fixed at 0.5 wt% of cement. The total content of the fine aggregate including standard sand and AIS sludge was also fixed at twice the weight of cement. The replacement ratio of the sludge to the standard sand was varied from 0 to 40 wt% of the cement. The mixing procedure of mortars with the AIS sludge was as follows: Water, superplasticizer, and fine aggregates (standard sand and AIS sludge) were mixed for 1 min in order to improve the dispersion of the sludge particles [18]. Cement powder was then

Table 1
Chemical composition of OPC and AIS sludge.

Chemical composition (%)	OPC	AIS sludge
CaO	60.3	0.4
SiO_2	20.4	97.5
Al_2O_3	4.6	0.7
TiO_2	0.3	0.6
Na_2O	0.2	–
MgO	3.3	–
Fe_2O_3	3.2	0.3
SO_3	2.3	–

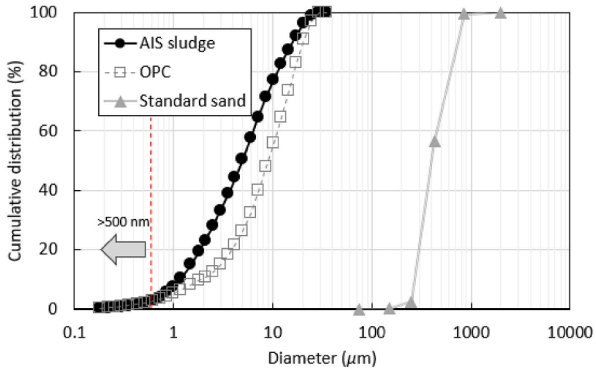

Fig. 1. Cumulative particle size distribution curves of OPC, standard sand, and AIS sludge.

Table 2
Mix proportion of mortars with AIS sludge (g).

	OPC	Water	Superplasticizer	Fine aggregate	
				Standard sand	AIS sludge
WS0	1000	410	5	2000	0
WS1				1900	100
WS2				1800	200
WS3				1700	300
WS4				1600	400

mixed for 3 min, and the mixture was cast into cubical molds with dimensions of 50 × 50× 50 mm^3. The samples were cured for designated periods at 25 ± 3 °C.

2.3. Methods

A compressive strength test was conducted according to the ASTM C109 using a universal testing machine (UTM) with a specification of 300 kN (RT-M-003-30PC, Ramt Co., Ltd.). The crosshead speed applied in the tests was fixed at 0.6 mm/min. The setting behavior of mortars with AIS sludge was measured by the penetration resistance test according to ASTM C403. A mixture was put into a container, and the penetration resistance at designated time intervals was measured by standard needles. In the test, the initial and final setting times are defined when the penetration resistance reaches 3.5 MPa and 27.6 MPa, respectively.

The flowability of mortars with AIS sludge was measured according to ASTM C1437. The values of flow for each mixture in the present study were measured for 60 min. The pore characteristics of the mortars with AIS sludge were investigated by a mercury intrusion porosimetry (MIP) test (AutoporeIV, Micromeritics Instrument Corporation). The detection range of pores was from 0.003 to 1000 μm in diameter, while the maximum intrusion pressure used here was 414 MPa. The surface tension and contact angle were fixed at 0.485 N/m and 130°, respectively. For the MIP tests, samples were immersed in anhydrous ethanol at a designated period and put into a vacuum chamber to arrest additional hydration [19].

The electrostatic potential (ESP) of H_2O and SiO_2 calculations was conducted through density functional theory (DFT) method in $DMol^3$ module of the Material Studio 2022 [20]. The structure optimization of molecules was carried out based on Beck-Lee Yang Parr (BLYP) functional of the Generalize Gradient Approximation (GGA) and a double numerical plus polarization (DNP) basis set in $DMol^3$ [21,22]. The MD simulations was also performed by using $DMol^3$ module. A single H_2O molecule was placed on the SiO_2 structure, and canonical ensemble (NVT) dynamics at 300 K for 10 ps was conducted with fixing the volume of the cell as the converged values [23,24]. Herein, the massive generalized Gaussian moments (GGM) was applied as the thermostat, the time step for the MD simulation was set to 1 fs, and the Yoshida parameter was considered to be 3, respectively. The distance between two atomistic systems was measured based on the final NVT simulation result.

In order to estimate the overall trends of engineering properties in specimens, a facile machine learning technique based on experimental results with specimen variables was carried out. Herein, the genetic algorithm (GA)-based multigene symbolic regression algorithm was applied to build a model equation by learning the tendency between input and output data [25,26]. The basic input variables were considered as water/cement ratio (w/c) and AIS sludge/sand ratio (A/s). Based on the two input parameters, porosities larger or smaller than 50 nm were initially estimated (φ_I and φ_{II}), and the correlations among each variable, the compressive strength (σ_c), and the flowability (F) of the specimens were analyzed [27]. The configuration and principle of the GA are described in more detail in the literature, and Fig. 2 shows a conceptual diagram of the corresponding approach considered in this study.

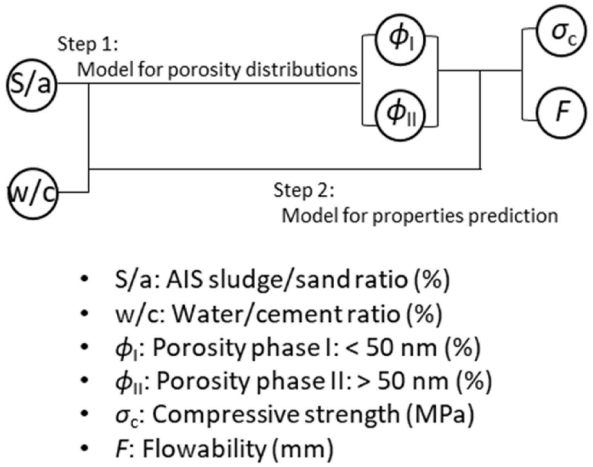

Fig. 2. Schematic illustrations of data-driven model for prediction of material properties.

3. Results

3.1. Compressive strength

Fig. 3 showed the compressive strength results of the mortars with AIS sludge at 3 days and 28 days. The test results indicated that the compressive strength of the mortars with the sludge at 3 days increased when the replacement ratio of the sludge was more than 10%. The corresponding compressive strengths of the WS0 and WS4 samples were 23.8 MPa and 38.1 MPa. That is, the compressive strength of the WS4 sample at 3 days increased up to approximately 59% compared to that of the WS0 sample. The compressive strength of the mortars at 28 days also increased when the replacement ratio of the sludge was 20 wt% (WS0 = 27.08 MPa, WS1 = 20.44 MPa, WS2 = 39.90 MPa, WS3 = 41.05 MPa, WS4 = 42.14 MPa). While the compressive strength of the WS3 and WS4 samples was similar to that of the WS2 sample. The compressive strength increased over WS0 in all cases except for the WS1 specimen. The compressive strength at 3 days increased by 32.9, 48.7, and 59.8% for WS2, WS3, and WS4 over WS0, and those at 28 days increased by 47.3, 51.6, and 55.6%, respectively. WS1 was the only specimen to show a decrease in compressive strength compared to the control specimen. The compressive strength of WS1 decreased by 4.7% at 3 days and by 24.5% at 28 days compared to WS0.

3.2. Flowability

Fig. 4 showed the flowability and flow loss of the mortars with AIS sludge within 60 min. In Fig. 4(a), the test results indicated that the flow values of mortars at 10 min were analogous when the replacement ratio of the sludge was lower than 30%, while that of the WS4 sample was clearly reduced. The flow value of the WS0, WS1, WS2, WS3, and WS4 samples at 10 min were 216 mm, 214 mm, 229 mm, 212 mm, and 187 mm, respectively. The flow values were reduced in all samples with increasing time. In particular, as shown in Fig. 4(b), the flow loss of the mortars with sludge at 20 min significantly increased compared to that of the WS0 sample. Furthermore, the increase in the flow loss of mortars with the sludge at 60 min was greater than that of the WS0 sample. The flow loss value of the WS0, WS1, WS2, WS3, and WS4 samples at 60 min were 11.5%, 21.96%, 23.58%, 29.72%, and 26.20%, respectively. At 60 min, the increase in flow loss WS4 was measured to be 26% over WS0.

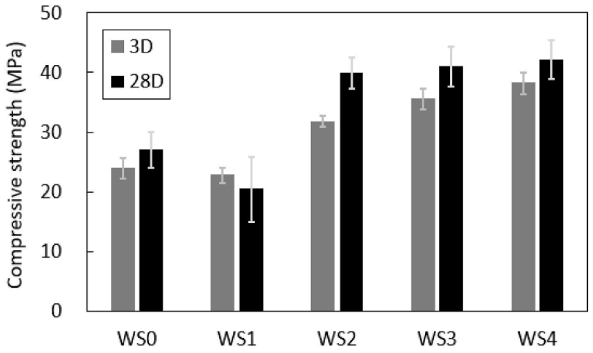

Fig. 3. Compressive strength results of mortars with AIS sludge at 3 days and 28 days.

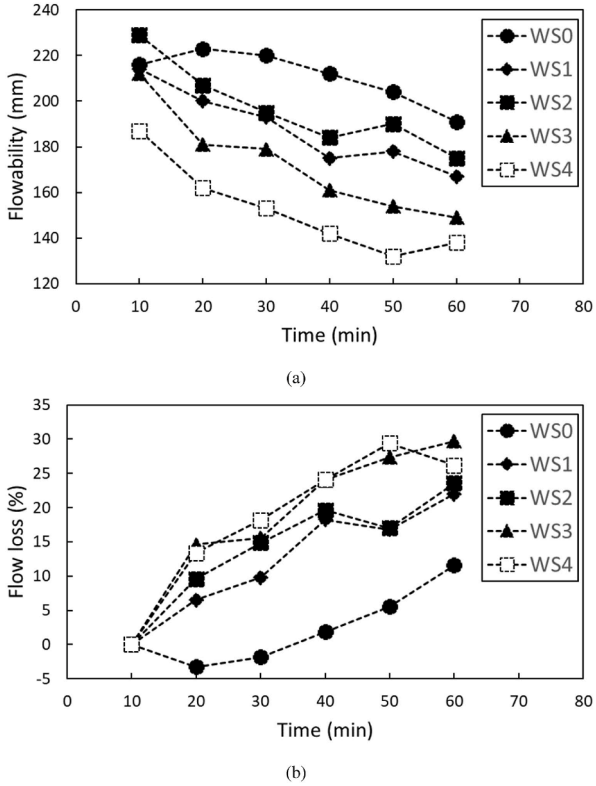

Fig. 4. (a)Flowability and (b) flow loss of mortars with AIS sludge within 60 min..

3.3. Penetration resistances

Fig. 5 showed the penetration resistances in the mortars with AIS sludge. The initial setting time of the mortars with a sludge of more than 20% was reduced compared to that of the WS0 sample. The initial setting time of the WS0 sample was 7.8 h, while those of the WS1, WS2, WS3, and WS4 samples were 9.9, 6.8, 6.1, and 8.2 h respectively. The WS1 sample reached the initial setting late compared to the WS0 sample. In contrast, the final setting time in all samples with the sludge was clearly reduced compared to that of the WS0 sample. The WS0 sample reached the final at 14.7 h, while the mortars with sludge reached the final setting within 14 h. The final setting times of the WS1, WS2, WS3, and WS4 samples were 13.8, 10.3, 10.2, 11.7 h, respectively. It can be seen that the final setting time of the specimen was shortened from a minimum of 6% to a maximum of 30%. The WS4 sample reached the final setting late compared to the WS2 and WS3, despite the higher sludge content. This was attributable that the excess addition of the sludge inhibited the setting or formed a defect by agglomeration of them.

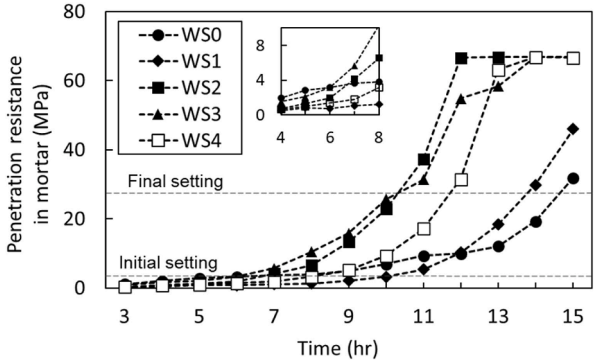

Fig. 5. Penetration resistances in mortars with AIS sludge.

3.4. MIP (mercury intrusion porosimetry)

Table 3 showed the total porosity of the mortars with AIS sludge at 3 days and at 28 days of curing. The total porosity of the mortars was mostly reduced as the curing progressed since the formation of hydrates densified the matrix. In addition, the total porosity of mortars at 3 days and 28 days of curing mostly tended to reduce due to the addition of sludge.

Fig. 6 showed the pore size distribution curves of the mortars with AIS at 3 days and 28 days of curing. Fig. 6(a) and (b) showed the pore size distribution curves of the mortars with AIS sludge at 3 days and at 28 days of curing, respectively. Herein, it was analyzed that the critical pore diameters of the WS0, WS1, WS2, WS3, and WS4 samples at 3 days of curing were 50.3 nm, 50.3 nm, 40.2 nm, 32.3 nm, and 32.2 nm, respectively, while those of the WS0, WS1, WS2, WS3, and WS4 samples at 28 days of curing were 50.3 nm, 50.3 nm, 50.3 nm, 40.2 nm, 32.3 nm, respectively. The critical pore size corresponds to the highest point in the pore size distribution curve [28]. The critical pore size was similar regardless of the curing period, while the pore size was reduced when the replacement ratio of the sludge was more than 20%. Meanwhile, the threshold pore sizes of the WS0, WS1, WS2, WS3, and WS4 samples at 3 days of curing were 77.1 nm, 77.1 nm, 77.1 nm, 62.4 nm, 62.4 nm, respectively, while those of the WS0, WS1, WS2, WS3, WS4 samples at 28 days of curing were 77.1 nm, 77.1 nm, 77.09 nm, 62.4 nm, 50.3 nm, respectively. The threshold pore size in the previous studies was defined as the last reflection point in the pore size distribution curves [28,29]. The threshold pore size of mortars in the present study was not significantly affected by curing periods. The reduction in the threshold pore size was observed when the replacement ratio of the sludge was more than 30%.

Fig. 7 showed the percentage of the pore volume of the mortars with AIS sludge at 3 days and at 28 days of curing. The test results indicated that the percentage of the pores with a size lower than 10 nm regardless of curing periods mostly tended to increase as the replacement ratio of the sludge increased. The percentage of the pores with a size between 10 nm and 50 nm also increased as the replacement ratio of the sludge increased. In contrast, the percentage of the pores with a size larger than 50 nm was reduced as the replacement ratio of the sludge increased. At 28 days, the porosity of >10 nm was 19, 20, 25, 26, and 24%, with WS1 through WS4 specimens increasing by 5.3, 31.6, 36.8, and 26.3%, respectively, compared to WS0. On the other hand, the porosity of <15,000 nm were 22, 23, 20, 11, and 13%, with WS2, WS3, and WS4 specimens decreasing by 9.1, 50.0, and 40.1%, respectively, compared to WS0, except for a slight increase of 4.5% for WS1 specimen.

Table 3
Total porosity of mortars with AIS sludge at 3 days and at 28 days of curing.

Sample	Total porosity (%)	
	3 days	28 days
WS0	23.6	21.0
WS1	32.3	19.7
WS2	19.3	17.0
WS3	22.8	25.9
WS4	17.5	17.9

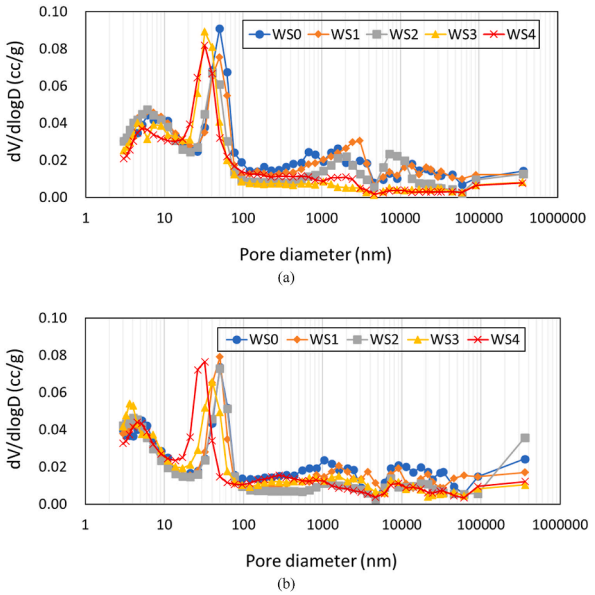

Fig. 6. Pore size distribution curves of mortars with AIS sludge at (a) 3 days and (b) 28 days of curing.

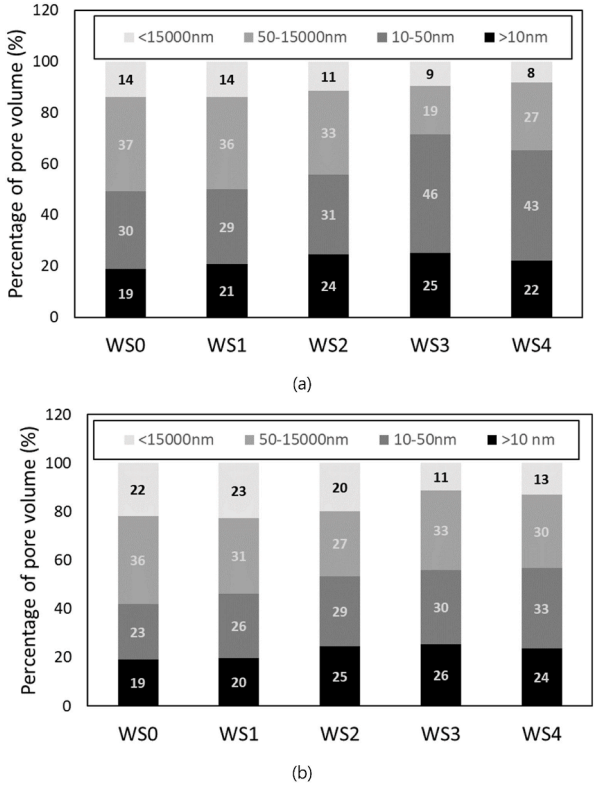

Fig. 7. Percentage of pore volume of mortars with AIS sludge at (a) 3 days and (b) 28 days of curing.

3.5. DFT (density functional theory) and MD (molecular dynamics)

Fig. 8 showed the DFT and MD simulation results of H_2O and SiO_2 molecules. The ESP distributions were represented in Fig. 8(a), indicating the positively and negatively charged regions of molecules. With the identical scale, it was analyzed that the O atom of the water molecule has a relatively negative charge, while the H atom has a positive charge. It can be seen from the figure that the SiO_2 structure has a positive charge overall. Hence, it was presumed that their opposite electrostatic potentials induce attraction between the two components [22]. Fig. 8(b) showed the MD trajectories of a single H_2O molecule and SiO_2 structure. As the simulation time proceeds, it was predicted that the H_2O gradually approach the SiO_2 surface. The distance between the H_2O and SiO_2 was narrowed to 1.874 Å, but it falls back somewhat over time. Even with continuous MD simulation, the H_2O hovered around the SiO_2 layer at about 1.8–2.3 Å. It was analyzed that the distribution of various electrostatic forces constituting the two molecules places a certain distance from each other.

3.6. GA (genetic algorithm)

Fig. 9 represents the compressive strength and flowability calculated through the GA-based approach. Since there is merely S/a as a variable parameter in the relationship between mix ratio and porosity amount, the equations for φ_1 and φ_2 were led as follows: $\varphi_1 = -0.63(S/a) + 0.56$; $\varphi_2 = 1 - \varphi_1$, where S/a denotes the ratio of AIS sludge and fine aggregate (sand); φ_1 and φ_2 mean the volume fraction of porosities larger and smaller than 50 nm, respectively. The equation that can predict the compressive strength according to the input values (S/a, w/c, φ_1, and φ_2) through the GA approach is developed and described as follows: $\sigma_c = 6.7 \cos(\varphi_1) - 1.82\varphi_1 + 124.5$, where σ_c denotes the compressive strength of the specimen. In addition, the flowability of specimens can be predicted by the derived equation: $F = -0.4\varphi_2 \sin(S/a) + 9.6 \cos(\varphi_1) + 208$. It was calculated that the root mean square (RMS) training set error and R^2 values for σ_c are 3.68 and 0.85; and the RMS and R^2 values for F are calculated as: 4.18 and 0.92, respectively.

4. Discussion

The effects of additives on the mechanical properties of cementitious materials can be divided into two groups. A general effect is the filler effect that the additives added to cementitious materials fill the pores in the matrix, while another effect is the nucleation seeding that the additives act as a nucleation site [30–32]. It has been reported in previous studies that the particle size of additives significantly affected the hydration evolution of cementitious materials since the particles of the size below 500 nm could act as a nucleation site for the formation of hydrates [33–36]. A part of the AIS sludge in the present study consisted of the particles lower than 500 nm as shown in Fig. 1. The proportion of the particles lower than 500 nm was approximately 1.9% of the sludge.

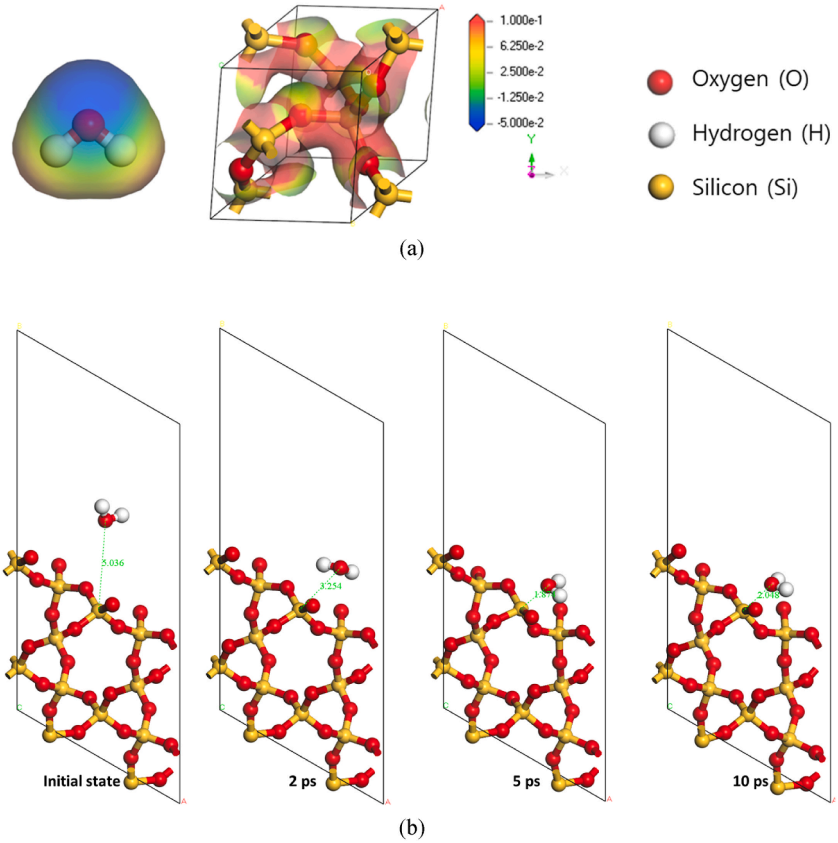

Fig. 8. (a) The electrostatic potential distributions and (b) the MD trajectories of H_2O and SiO_2 molecules.

In this context, it can be inferred from the flow test results that the addition of the AIS sludge promoted the nucleation of the hydrates. The flow loss in the tests increased when the sludge was added. The flowability of cementitious materials is generally affected by the free water in the mixture [37]. The water in a cementitious matrix can exist in three types affecting flowability. They are the free water, the adsorbed layer water, and the filling water [38]. The free water enables the separation of particles, thereby contributing to an increase in flowability. The free water in the hydration process of cementitious materials is consumed, forming hydrates such as C–S–H and ettringite phases [39]. The formula of the C–S–H phase being the major hydrate of cementitious materials is reportedly analogous to the 11 Å-Tobermorite ($Ca_{2.25}$ $[Si_3O_{7.5}(H)_{1.5}]$ • $8H_2O$), and the phase could be formed within the first minutes when adding nucleation seeds [39,40]. The formation of ettringite ($Ca_6Al_2(SO_4)_3(OH)_{12}{\cdot}26H_2O$) is involved in the dissolution of C_3A phases in OPC powder and sulfate ions. The dissolution of the C_3A phase in previous studies was initiated upon contacting water until approximately 10 h, leading to the formation of ettringite consuming sulfate ions [41,42]. That is, one part of the flow loss when adding the sludge to mortars could be induced by the promotion of hydration. Besides, the addition of the sludge possibly increased the adsorbed layer water which could negatively affect the flowability. The sludge particles could adsorb more water on the surface compared to OPC and standard sand since the particle size of the sludge was smaller than those of others. It is well known that fine particles with a large specific surface area could adsorb more water on the surface [38]. Hence, another part of the flow loss when adding the sludge to mortars could be induced by an increase in the adsorbed layer water on the surface of the sludge. The present DFT and MD simulation results help us to display ESP map and trajectories of atomistic systems, and to understand the mechanism of adsorbed layer water on the surface of the sludge. Upon mixing, the more H_2O molecules were attached to the sludge surface owing to the charge-transfer interaction, and the sludge were expected to act as water carriers.

The initial and final setting times were reduced when adding the sludge. The effect of the sludge addition on the reduction in the initial setting time in the penetration resistance tests was not significant, while that on the final setting time was significant. Yuan et al. reported that the higher the yield stress of the mixture is, the smaller the flow is [43]. The yield stress could depend on the hydration in the mixture of cementitious materials [43]. It has been reported in previous studies that the addition of nucleation seeds significantly accelerated the hydration between 8 h and 13 h [44–46]. Thus, it can be inferred from the previous studies that the promotion of hydration between 8 and 13 h significantly progressed, leading to the difference in the final setting time of the mortars with AIS sludge.

The total porosity, and critical and threshold pore size results indicated that the addition of the sludge contributed to filling the pores in the cementitious matrix when the replacement ratio of the sludge added to mortars was more than 20 wt%. The critical pore size is associated with the transmissivity of the cementitious matrix [28]. The maximum percolation of chemical species in the cemen-

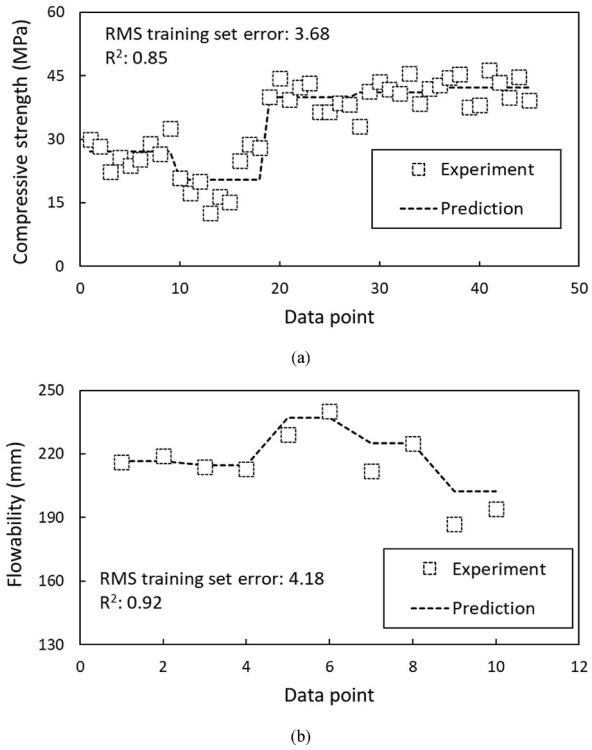

Fig. 9. Comparisons between experimental data and predictions for (a) compressive strength and (b) flowability.

titious matrix occurs in the interconnected pores [47]. The threshold pore size represents the minimum size of continuous channels through the cementitious matrix [28,29]. That is, the reduction in the critical and threshold pore sizes in the mortars with AIS sludge could improve the durability [48,49].

The percentage of pores with a diameter of lower than 10 nm in the pore size distribution curves increased as the replacement ratio of the sludge increased. The pore size may be involved in the presence of the C–S–H phases. Wenzel et al. reported that the average diameter of the honeycomb pore structure in the C–S–H phase was approximately 2–10 nm [50]. Naber et al. also reported that the gel pore size in the C–S–H phase was approximately 8.1 nm [51]. Furthermore, the pores with a diameter ranging from 10 nm to 50 nm was reportedly involved in the medium capillary pores or the pores between interhydrates [52]. The medium capillary pores and the pores between interhydrates are one of the indices responsible for the strength of cementitious materials [52]. The percentage of the pores with a diameter ranging from 10 nm to 50 nm in the present study tended to increase as the replacement ratio of the AIS sludge increased. Overall, the addition of the AIS sludge probably contributed to the hydration reaction, thereby leading to an increase in the hydrates of mortars. Meanwhile, the percentage of the pores with a diameter of more than 50 nm was reduced as the replacement ratio of the AIS sludge increased. The pore size was classified into large capillary pores that could act as a defect site [53]. Hence, it could be implied that the addition of the sludge filled the pores in the range of large capillary pores, reducing the defect of samples.

The compressive strength results are consistent with the MIP test results. The compressive strength of mortars at 3 days and 28 days was not clearly improved when the replacement ratio of the sludge was 10%. The pore characteristics of the WS10 sample in the present study were analogous to that of the WS0 sample. The clear difference between the WS0 and WS10 samples was merely observed in flow tests. The flow loss of the WS10 sample with reaction time was higher than that of the WS0 sample. This was attributable to the adsorbed layer water on the surface of the sludge. The compressive strength of mortars significantly increased when the replacement ratio of the sludge was 20%. Referring to the test results in the present study, the hydration of mortars was clearly promoted in the WS20 sample and the matrix was densified by filling effect. In detail, the initial and final setting times were reduced, the pores involved in the presence of hydrates increased, and the pores involved in the defect site were reduced. However, the aforementioned effects induced by adding the sludge tended to be mitigated when the replacement ratio of the sludge was more than 30%. As a result, the compressive strength of the WS3 and WS4 samples was analogous to that of the WS2 sample. That is, there was an upper limit on the replacement ratio of the sludge in order to the promotion of hydration due to the supply of nucleation seeds. It has been reported in previous studies that the upper limit of the content for the nucleation seeding ranged from 1.0 to 5.0 wt% [54,55]. The effects of the hydration promotion were mitigated when exceeding the replacement ratio [54,55]. In contrast, the filling effect on the defect site in the range of more than 15, 000 nm was clear when the replacement ratio of the sludge was more than 30%. In summary, the amalgamation of augmenting the filler contribution and constraining the promotion of hydration, specifically when the substitu-

tion proportion of the sludge exceeded 30%, may potentially account for the observed outcomes pertaining to the compressive strength.

From the machine learning-based simulation results, it is worth noting that the present GA approach automatically identifies the most influential variables and constructs the equation. Herein, it was estimated that the parameter with the highest influence on σ_c is φ_1, and the F was affected by parameters of φ_1 and φ_2. In addition, it had a fairly high degree of regularity in the experimental data, and it resulted in a high degree of agreement.

5. Conclusions

The effects of the AIS sludge addition on the physicomechanical properties of mortars in the present study were investigated. The independent variable was the replacement ratio of the sludge to fine aggregates. The physicomechanical properties of the mortars with the sludge were investigated via flow, penetration resistance, pore characterization, and compressive strength tests. The main results obtained in the present study were as follows.

(1) The compressive strength of the mortars with the sludge increased when the replacement ratio of the sludge was more than 20%. The compressive strength of the sample with the sludge of 40% increased up to 59% compared to that of the sample without the sludge.
(2) The addition of the sludge to mortars reduced the flowability. The flow loss of the samples with the sludge at 20 min significantly increased compared to that of the sample without the sludge.
(3) The initial setting time of the samples with the sludge tended to be slightly reduced compared to the sample without the sludge. While the final setting time was clearly reduced when the replacement ratio of the sludge was in the range of 20–30%.
(4) The addition of the sludge to the samples tended to reduce the total porosity, and critical and threshold pore sizes. In addition, the use of sludge contributed to an increase in the pores with a size involved in the presence of hydrates and to a reduction in the pores with a size acting as a defect site. This is considered to have contributed to the improvement of compressive strength, in line with the result (1).
(5) The DFT and MD simulations reveled that H_2O and SiO_2 molecules had opposite ESPs, and mutual attraction enhanced. It was also analyzed by GA that the compressive strength was mainly affected by the distribution of voids of 50 nm or less.

Overall, it can be concluded that the addition of the AIS sludge contributed to the promotion of the hydration and densification of the matrix, thereby improving the mechanical properties. The analysis of the relationship based on the compression strength and MIP results can empirically substantiate the improvement hypothesis. Through computational analyses, the material mechanisms and symbolic model formula for mix ratio of specimens was proposed.

Credit author statement

G. M. Kim: Writing – original draft, Conceptualization; Jaesuk Choi: Data curation, Investigation; Jinho Bang: Data curation, Investigation; Jongwon Jung: Data curation; S. W. Park: Validation, Formal analysis; Beomjoo Yang: Writing – review and editing, Supervision.

Declaration of competing interest

We wish to confirm that there are no known conflicts of interest associated with this publication and there has been no significant financial support for this work that could have influenced its outcome.

We confirm that the manuscript has been read and approved by all named authors and that there are no other persons who satisfied the criteria for authorship but are not listed. We further confirm that the order of authors listed in the manuscript has been approved by all of us.

We confirm that we have given due consideration to the protection of intellectual property associated with this work and that there are no impediments to publication, including the timing of publication, with respect to intellectual property. In so doing we confirm that we have followed the regulations of our institutions concerning intellectual property.

We understand that the Corresponding Author is the sole contact for the Editorial process. He/she is responsible for communicating with the other authors about progress, submissions of revisions and final approval of proofs. We confirm that we have provided a current, correct email address which is accessible by the corresponding author byang@chuyngbuk.ac.kr (B·Y).

Data availability

No data was used for the research described in the article.

Acknowledgments

This work was supported by the Industrial Strategic technology development program-Development of manufacturing technology of hardened cement with carbonation curing (RS-2022-00155662, Development of manufacturing and application technology of 1000 ton/year class hardened cement with carbonation curing) funded by the Ministry of Trade, industry & Energy (MOTIE, Korea). In addition, this work was supported by a National Research Foundation of Korea (NRF) grant funded by the Korean government (MSIT) (2022R1A4A3029737).

References

[1] M. Amran, S.-S. Huang, A.M. Onaizi, N. Makul, H.S. Abdelgader, T. Ozbakkaloglu, Recent trends in ultra-high performance concrete (UHPC): current status, challenges, and future prospects, Construct. Build. Mater. 352 (2022) 129029.
[2] K. Mojapelo, W. Kupolati, J. Ndambuki, E. Sadiku, I. Ibrahim, Utilization of wastewater sludge for lightweight concrete and the use of wastewater as curing medium, Case Stud. Constr. Mater. 15 (2021) e00667.
[3] D. Katerusha, Investigation of the optimal price for recycled aggregate concrete—an experimental approach, J. Clean. Prod. 365 (2022) 132857.
[4] J.I. Bhatty, A. Malisci, I. Iwasaki, K.J. Reid, Sludge ash pellets as coarse aggregates in concrete, Cem. Concr. Aggregates 14 (1) (1992).
[5] J. Chiou, K.-S. Wang, C.-H. Chen, Y.-T. Lin, Lightweight aggregate made from sewage sludge and incinerated ash, Waste Manag. 26 (12) (2006) 1453–1461.
[6] C. Lam, J.P. Barford, G. McKay, Utilization of incineration waste ash residues in Portland cement clinker, Chem. Eng. 21 (2010) 757–762.
[7] C.J. Lynn, R.K. Dhir, G.S. Ghataora, R.P. West, Sewage sludge ash characteristics and potential for use in concrete, Construct. Build. Mater. 98 (2015) 767–779.
[8] C. Fontes, M. Barbosa, R. Toledo Filho, J. Goncalves, Potentiality of sewage sludge ash as mineral additive in cement mortar and high performance concrete, Intern. RILEM Confe. Use Recycl. Mater. Build. Struct. (2004) 797–806.
[9] Z. Chen, J.S. Li, C.S. Poon, Combined use of sewage sludge ash and recycled glass cullet for the production of concrete blocks, J. Clean. Prod. 171 (2018) 1447–1459.
[10] M. Allam, E. Bakhoum, G. Garas, Re-use of granite sludge in producing green concrete, J. Eng. Appl. Sci. 9 (12) (2014) 2731–2737.
[11] D. Nakic, Environmental evaluation of concrete with sewage sludge ash based on LCA, Sustain. Prod. Consum. 16 (2018) 193–201.
[12] J.J. Thomas, J.J. Biernacki, J.W. Bullard, S. Bishnoi, J.S. Dolado, G.W. Scherer, A. Luttge, Modeling and simulation of cement hydration kinetics and microstructure development, Cement Concr. Res. 41 (12) (2011) 1257–1278.
[13] H. Wang, H. Shin, Recent studies on the multiscale models for predicting fracture toughness of polymer nanocomposites, Multiscale Sci. Eng. 4 (1–2) (2022) 1–9.
[14] H.-K. Kim, Y. Lim, M. Tafesse, G. Kim, B. Yang, Micromechanics-integrated machine learning approaches to predict the mechanical behaviors of concrete containing crushed clay brick aggregates, Construct. Build. Mater. 317 (2022) 125840.
[15] S. Wan, X. Zhou, M. Zhou, Y. Han, Y. Chen, J. Geng, T. Wang, S. Xu, Z. Qiu, H. Hou, Hydration characteristics and modeling of ternary system of municipal solid wastes incineration fly ash-blast furnace slag-cement, Construct. Build. Mater. 180 (2018) 154–166.
[16] Q. Han, Y. Yang, J. Zhang, J. Yu, D. Hou, B. Dong, H. Ma, Insights into the interfacial strengthening mechanism of waste rubber/cement paste using polyvinyl alcohol: experimental and molecular dynamics study, Cement Concr. Compos. 114 (2020) 103791.
[17] Y. Shin, J.G. Jang, J. Choi, G. Jun, C. Park, G. Kim, B. Yang, Utilization of artificial interior stone sludge as fine aggregate in controlled low-strength material (CLSM), J. Build. Eng. 71 (2023) 106441.
[18] G. Kim, S. Park, G. Ryu, H.-K. Lee, Electrical characteristics of hierarchical conductive pathways in cementitious composites incorporating CNT and carbon fiber, Cement Concr. Compos. 82 (2017) 165–175.
[19] H. Wang, X. Liu, S. Wang, S. Zhou, T. Zang, L. Dai, S. Ai, Hydrophobic kenaf straw core for biomass-based cement mortar with excellent mechanical properties, Mater. Chem. Phys. 267 (2021) 124594.
[20] B. Delley, From molecules to solids with the DMol 3 approach, J. Chem. Phys. 113 (18) (2000) 7756–7764.
[21] C. Lee, W. Yang, R.G. Parr, Development of the Colle-Salvetti correlation-energy formula into a functional of the electron density, Phys. Rev. B 37 (2) (1988) 785.
[22] C.B. Kim, K.B. Jeong, B.J. Yang, J.W. Song, B.C. Ku, S. Lee, S.K. Lee, C. Park, Facile supramolecular processing of carbon nanotubes and polymers for electromechanical sensors, Angew. Chem. 129 (51) (2017) 16398–16403.
[23] B. Yang, H. Shin, H.-K. Lee, H. Kim, A combined molecular dynamics/micromechanics/finite element approach for multiscale constitutive modeling of nanocomposites with interface effects, Appl. Phys. Lett. 103 (24) (2013) 241903.
[24] I. Jeon, T. Yun, S. Yang, Classical, coarse-grained, and reactive molecular dynamics simulations on polymer nanocomposites, Multiscale Sci. Eng. 4 (4) (2022) 161–178.
[25] D.P. Searson, D.E. Leahy, M.J. Willis, Predicting the toxicity of chemical compounds using GPTIPS: a free genetic programming toolbox for MATLAB, Intell. Control Comp. Eng. (2011) 83–93.
[26] Y. Shin, H.M. Park, J. Park, H. Cho, S.-E. Oh, S.-Y. Chung, B. Yang, Effect of polymer binder on the mechanical and microstructural properties of pervious pavement materials, Construct. Build. Mater. 325 (2022) 126209.
[27] D. Jang, J. Bang, H. Yoon, J. Seo, J. Jung, J.G. Jang, B. Yang, Deep learning-based LSTM model for prediction of long-term piezoresistive sensing performance of cement-based sensors incorporating multi-walled carbon nanotube, Comput. Concr. 30 (5) (2022) 301–310.
[28] Y. Chen, F. Al-Neshawy, J. Punkki, Investigation on the effect of entrained air on pore structure in hardened concrete using MIP, Construct. Build. Mater. 292 (2021) 123441.
[29] S. Diamond, D. Winslow, A mercury porosimetry study of the evolution of porosity in Portland cement, J. Mater. 5 (3) (1970) 564–585.
[30] M.I. Khan, R. Siddique, Utilization of silica fume in concrete: review of durability properties, Resources, Conserv. Recycl. 57 (2011) 30–35.
[31] L. Wang, D. Zheng, S. Zhang, H. Cui, D. Li, Effect of nano-SiO2 on the hydration and microstructure of Portland cement, Nanomaterials 6 (12) (2016) 241.
[32] M. Balapour, A. Joshaghani, F. Althoey, Nano-SiO2 contribution to mechanical, durability, fresh and microstructural characteristics of concrete: a review, Construct. Build. Mater. 181 (2018) 27–41.
[33] G. Kim, F. Naeem, H. Kim, H.-K. Lee, Heating and heat-dependent mechanical characteristics of CNT-embedded cementitious composites, Compos. Struct. 136 (2016) 162–170.
[34] E. John, T. Matschei, D. Stephan, Nucleation seeding with calcium silicate hydrate–A review, Cement Concr. Res. 113 (2018) 74–85.
[35] M.K. Ardoğa, S.T. Erdoğan, M. Tokyay, Effect of particle size on early heat evolution of interground natural pozzolan blended cements, Construct. Build. Mater. 206 (2019) 210–218.
[36] J. Yang, M. Yang, X. He, M. Ma, M. Fan, Y. Su, H. Tan, Green reaction-type nucleation seed accelerator prepared from coal fly ash ground in water environment, Construct. Build. Mater. 306 (2021) 124840.
[37] M. Zhao, X. Zhang, Y. Zhang, Effect of free water on the flowability of cement paste with chemical or mineral admixtures, Construct. Build. Mater. 111 (2016) 571–579.
[38] F.J. Luo, L. He, Z. Pan, W.H. Duan, X.L. Zhao, F. Collins, Effect of very fine particles on workability and strength of concrete made with dune sand, Construct. Build. Mater. 47 (2013) 131–137.
[39] J.J. Thomas, J.J. Chen, H.M. Jennings, D.A. Neumann, Ca– OH bonding in the C– S– H gel phase of tricalcium silicate and white Portland cement pastes measured by inelastic neutron scattering, Chem. Mater. 15 (20) (2003) 3813–3817.
[40] D. Kong, S. Huang, D. Corr, Y. Yang, S.P. Shah, Whether do nano-particles act as nucleation sites for CSH gel growth during cement hydration? Cement Concr. Compos. 87 (2018) 98–109.
[41] D. Jansen, F. Goetz-Neunhoeffer, C. Stabler, J. Neubauer, A remastered external standard method applied to the quantification of early OPC hydration, Cement Concr. Res. 41 (6) (2011) 602–608.
[42] D. Jansen, C. Naber, D. Ectors, Z. Lu, X.-M. Kong, F. Goetz-Neunhoeffer, J. Neubauer, The early hydration of OPC investigated by in-situ XRD, heat flow calorimetry, pore water analysis and 1H NMR: learning about adsorbed ions from a complete mass balance approach, Cement Concr. Res. 109 (2018) 230–242.
[43] Q. Yuan, Z. Li, D. Zhou, T. Huang, H. Huang, D. Jiao, C. Shi, A feasible method for measuring the buildability of fresh 3D printing mortar, Construct. Build. Mater. 227 (2019) 116600.
[44] J. Wang, C. Qian, J. Qu, J. Guo, Effect of lithium salt and nano nucleating agent on early hydration of cement based materials, Construct. Build. Mater. 174 (2018) 24–29.
[45] P. Feng, H. Chang, X. Liu, S. Ye, X. Shu, Q. Ran, The significance of dispersion of nano-SiO2 on early age hydration of cement pastes, Mater. Des. 186 (2020) 108320.

[46] C. Luan, Y. Zhou, Y. Liu, Z. Ren, J. Wang, L. Yuan, S. Du, Z. Zhou, Y. Huang, Effects of nano-SiO2, nano-CaCO3 and nano-TiO2 on properties and microstructure of the high content calcium silicate phase cement (HCSC), Construct. Build. Mater. 314 (2022) 125377.
[47] P. Pipilikaki, M. Beazi-Katsioti, The assessment of porosity and pore size distribution of limestone Portland cement pastes, Construct. Build. Mater. 23 (5) (2009) 1966–1970.
[48] M. O'Farrell, S. Wild, B. Sabir, Pore size distribution and compressive strength of waste clay brick mortar, Cement Concr. Compos. 23 (1) (2001) 81–91.
[49] H.N. Atahan, O.N. Oktar, M.A. Taşdemir, Effects of water–cement ratio and curing time on the critical pore width of hardened cement paste, Construct. Build. Mater. 23 (3) (2009) 1196–1200.
[50] O. Wenzel, M. Schwotzer, E. Müller, V.S.K. Chakravadhanula, T. Scherer, A. Gerdes, Investigating the pore structure of the calcium silicate hydrate phase, Mater. Char. 133 (2017) 133–137.
[51] C. Naber, F. Kleiner, F. Becker, L. Nguyen-Tuan, C. Rößler, M.A. Etzold, J. Neubauer, CSH pore size characterization via a combined nuclear magnetic resonance (NMR)–scanning electron microscopy (SEM) surface relaxivity calibration, Materials 13 (7) (2020) 1779.
[52] D. Silva, V. John, J. Ribeiro, H. Roman, Pore size distribution of hydrated cement pastes modified with polymers, Cement Concr. Res. 31 (8) (2001) 1177–1184.
[53] J. Sun, L. Tian, Z. Yu, Y. Zhang, C. Li, G. Hou, X. Shen, Studies on the size effects of nano-TiO2 on Portland cement hydration with different water to solid ratios, Construct. Build. Mater. 259 (2020) 120390.
[54] Y. Qing, Z. Zenan, K. Deyu, C. Rongshen, Influence of nano-SiO2 addition on properties of hardened cement paste as compared with silica fume, Construct. Build. Mater. 21 (3) (2007) 539–545.
[55] M. Oltulu, R. Şahin, Effect of nano-SiO2, nano-Al2O3 and nano-Fe2O3 powders on compressive strengths and capillary water absorption of cement mortar containing fly ash: a comparative study, Energy Build. 58 (2013) 292–301.